


Relationship between volcanic ash fallouts and seismic tremor: quantitative assessment of the 2015 eruptive period at Cotopaxi volcano, Ecuador

Benjamin Bernard¹  · Jean Battaglia² · Antonio Proaño¹ · Silvana Hidalgo¹ · Francisco Vásconez¹ · Stephen Hernandez¹ · Mario Ruiz¹

Received: 8 June 2016 / Accepted: 13 October 2016 / Published online: 24 October 2016
© Springer-Verlag Berlin Heidelberg 2016

Abstract Understanding the relationships between geophysical signals and volcanic products is critical to improving real-time volcanic hazard assessment. Thanks to high-frequency sampling campaigns of ash fallouts (15 campaigns, 461 samples), the 2015 Cotopaxi eruption is an outstanding candidate for quantitatively comparing the amplitude of seismic tremor with the amount of ash emitted. This eruption emitted a total of $\sim 1.2\text{E} + 9$ kg of ash ($\sim 8.6\text{E} + 5$ m³) during four distinct phases, with masses ranging from $3.5\text{E} + 7$ to $7.7\text{E} + 8$ kg of ash. We compare the ash fallout mass and the corresponding cumulative quadratic median amplitude of the seismic tremor and find excellent correlations when the dataset is divided by eruptive phase. We use scaling factors based on the individual correlations to reconstruct the eruptive process and to extract synthetic Eruption Source Parameters (daily mass of ash, mass eruption rate, and column height) from the seismic records. We hypothesize that the change in scaling factor through time, associated with a decrease in seismic amplitudes compared to ash emissions, is the result of a more efficient fragmentation and transport process. These results open the possibility of feeding numerical models with continuous geophysical data,

after adequate calibration, in order to better characterize volcanic hazards during explosive eruptions.

Keywords Cotopaxi · Ash fallout · Seismic tremor · Correlation · Ashgram

Introduction

Ash plumes and fallouts are the most common and widespread volcanic hazards during explosive eruptions and can seriously impact society at both local and global scales (Jenkins et al. 2015). Ash dispersal assessment is currently achieved through the use of volcanic ash transport and dispersal models coupled with numerical weather prediction models (Connor et al. 2001; Costa et al. 2006; Kratzmann et al. 2010; Collini et al. 2012). According to Bonadonna et al. (2012), the key Eruption Source Parameters needed to parameterize these models are: plume height, eruption mass, mass eruption rate (MER), total grain-size distribution, and the onset and end of an eruption. For real-time forecasts, general pre-defined parameters can be used to create dispersal scenarios (Mastin et al. 2009), but dedicated ones, based on ash fallouts characterization, significantly improve the simulation results (Parra et al. 2016).

Eruption mass and MER during explosive events are difficult to estimate in real-time due to the problem of accessing information on the whole particle-size spectrum (Bonadonna et al. 2012). Imagery (infrared/visual/ultraviolet), either ground-based or from satellites, provides only superficial information on the eruptive plume and are sensitive to cloud cover (Bonadonna et al. 2012, Dürig et al. 2015). Radar and LIDAR techniques allow collection of useful data on grain-size and mass transport rate but are not yet commonly used and present some logistical issues (Donnadieu 2012, Donnadieu et al. 2016 and references therein for a complete

Editorial responsibility: J. Taddeucci

Electronic supplementary material The online version of this article (doi:10.1007/s00445-016-1077-5) contains supplementary material, which is available to authorized users.

✉ Benjamin Bernard
bbernard@igepn.edu.ec

¹ Escuela Politécnica Nacional, Instituto Geofísico, Ladrón de Guevara E11-253 y Andalucía, 6to piso ed. Ing. Civil, Quito, Ecuador

² Laboratoire Magmas et Volcans, Université Blaise Pascal-CNRS-IRD, OPGC, 5, Rue Kessler, 63038 Clermont-Ferrand, France

review). Infrasound and pressure records have been used for estimating exit velocities and MER (Caplan-Auerbach et al. 2010; Matoza et al. 2013; Ripepe et al. 2013) but such studies are still scarce and require calibration. Seismology is the most commonly used method to monitor volcanic activity and since the early 90s relationships between seismic tremor and tephra production have been explored (McNutt 1994; Alparone et al. 2003; Prejean and Brodsky 2011; Andronico et al. 2013; Kumagai et al. 2015; and references therein). Nevertheless, due to the lack of accurate real-time data on ash emissions, it remains extremely difficult to quantitatively correlate them. Globally, multidisciplinary approaches coupling ash sampling, ground-based and satellite monitoring are necessary to improve model parameterizations.

Cotopaxi (5897 m, 0.677°S, 78.436°W, Fig. 1a) is one of the most active volcanoes in Ecuador with 5 major eruptive cycles since 1532 (Hall and Mothes 2008), including 13 significant eruptions with VEI ≥ 3 (Volcanic Explosivity Index, Newhall and Self 1982). The last significant eruption occurred in 1880 but the volcano was still active at the beginning of the twentieth century (Pistolesi et al. 2011). Since continuous seismic monitoring began at the volcano in 1986, shallow long-period (LP), volcano-tectonic (VT), and icequake activity have been a persistent presence at Cotopaxi. According to Ruiz et al. (1998), the majority of VT and LP activity between 1989 and 1997 is attributed to the hydrothermal system interacting with heat from shallow depths. Beginning in January 2001, a prolonged period of unrest, suggesting a new intrusion of magma, was characterized first by intense

swarms of LP events followed by a cascade VT events (Molina et al., 2008). This inferred intrusion is also supported by deformation data and modeling suggesting a $\sim 2E + 7 \text{ m}^3$ input of magma in the southwest flank of the summit between 2001 and 2002 (Hickey et al., 2015). In the ensuing years until April 2015, seismic activity was reduced to low-level intermittent LP activity that rarely exceeded 50 events per day.

The first objective of this paper is to present a quantitative assessment of the ash fallouts during the August–November 2015 eruptive period with a high sampling frequency in order to classify this eruption in terms of size and phenomenology. We then explore the relationship between the ash fallouts and the intense seismic tremor observed simultaneously. We provide a simple but robust statistical analysis of this relationship and use it to extract volcano-physical information from the seismic records. Finally, we discuss the meaning of the observed correlations in terms of source processes and hazard assessment.

Eruption chronicles

After 73 years of quiescence, Cotopaxi started a new eruption on August 14, 2015. Precursory seismic activity initiated as early as April and degassing during May according to the Instituto Geofísico de la Escuela Politécnica Nacional (IGEPN special reports, www.igepn.edu.ec, Hidalgo et al. 2016). This eruption lasted until the end of November and

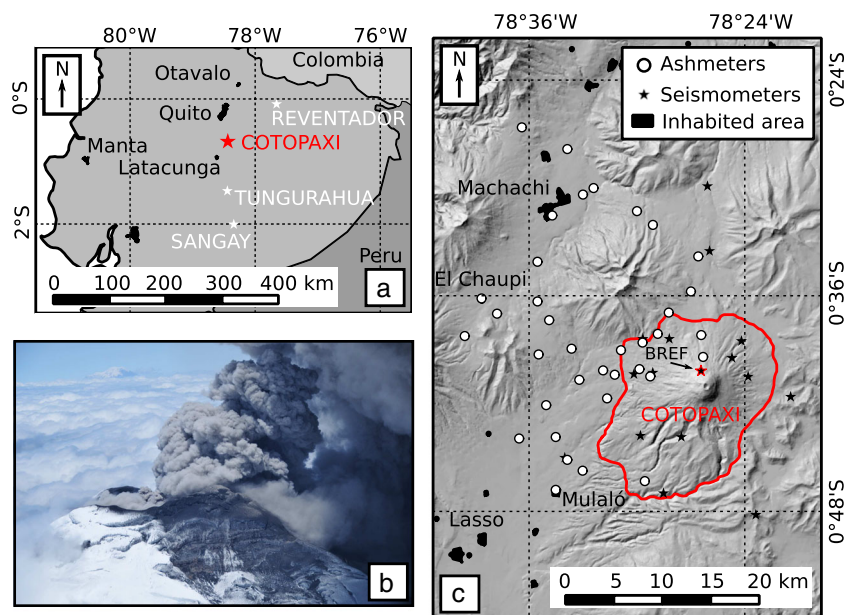


Fig. 1 a Location of Cotopaxi along with other currently active volcanoes (stars) in Ecuador (Tungurahua, Reventador, and Sangay). Main cities in black areas. b Typical low-energy, moderate-ash content, ~ 1 km-high ash emission at Cotopaxi during the second eruptive phase seen from the NNE (August 26, 2015). Note the ash deposit that covers

the northwestern and western flank of the volcano. c Location of the ashmeters (white circles) and seismic monitoring network (black stars) as of November 2015. Coordinates in WGS84 (zone 17 M). Red line around Cotopaxi corresponds to the perimeter of the volcano. Black star with red stroke corresponds to BREF seismic station

was divided into four phases based on the observed phenomenology using geophysical signals (seismic and acoustic), ground-based, airborne, and satellite imagery (visual and infrared). The first phase lasted 2 days (14–15/08); two explosions partially opened the system on August 14 (04:02 and 04:07 local time), producing ash clouds that rose ~7.8 km above the crater (Washington VAAC, www.ospo.noaa.gov). The explosive activity was mostly limited to the first day of the eruption with two more explosions at 13:45 and 16:02 (local time) producing ash clouds reaching up to 9.3 km above the crater. The eruptive products from the opening phase were only fallouts with almost exclusively ash and a small amount (<2 %) of fine lapilli (2–4 mm) in the proximal area. Few ballistic projectiles fell on the upper slopes of the volcano as described by climbers that were approaching the summit (~5400 m) during the first explosions. This phase was immediately followed by a second phase characterized by an increase of seismic tremor amplitude and vigorous ash emission reaching a maximum intensity in both parameters during the last week of August (Fig. 1b and Fig. 2). Then, the eruption gradually waned until the end of September. During this second phase (15/08–02/10), the eruptive plumes were typically smaller than 4 km high with low thermal anomalies (<200 °C). The volcano renewed ash emissions on October 2 accompanied by an increase of seismic tremor amplitude and <3 km-high plumes. During this third eruptive phase (02/10–04/11), the maximum intensity in seismic tremor and ash emission was reached around mid-October. At the beginning of this phase (02/10), a weak intermittent red glow was observed in the eruptive plume above the crater. This phenomenon was attributed to the reflection of an incandescent source in the upper conduit. This phase gradually waned until the beginning of November. Finally, a small ash

emission, categorized as a fourth phase (04/11–30/11), was registered during November with low-altitude (<2.5 km high) ash plumes.

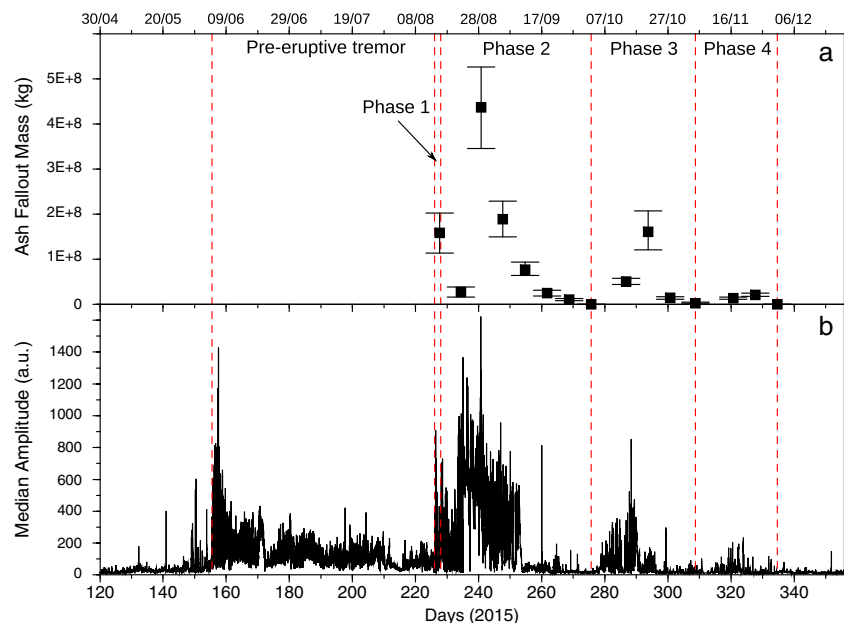
Since the beginning of the eruption, ash has been the only primary volcanic hazard disrupting air traffic and affecting communities located west and northwest of the volcano. Except from August 14, no explosions with ballistic projectiles were visually observed.

Data acquisition

Ash sampling and quantification

Fifteen field campaigns to collect and properly sample the emitted ash were performed between August 14 and November 30. Sampling techniques were diverse at first (roofs, solar panels, floors, buckets, homemade ashmeters) but were standardized after the third campaign by deploying homemade ashmeters. These ash collectors allow proper measurements of ash thickness and load (area density) for small deposits with minimum weathering effects (Bernard, 2013). The ashmeters used have a detection limit for thickness and load measurements of ~0.3 mm and ~0.5 g m⁻², respectively. Due to the small number of thickness measurements, we used the load (area density) for the fallout quantification. The proximal sampling network grew from 12 to 37 sample sites covering a total area of more than 600 km² (Fig. 1c). Ashmeters were also installed in several Ecuadorian cities (Quito, Conocoto, Latacunga, Manta, Otavalo, and Tababela) to detect the occurrence of ash fallout at distal places from the volcano. A total of 461 samples were collected (Online Resource 1), dried at 40 °C during 24 to 48 h in order to limit

Fig. 2 **a** Ash fallout mass per sampling campaign and **b** seismic tremor (median amplitude) at Cotopaxi volcano from April to December 2015, including pre-eruptive tremor and eruptive phases. Error bars for ash fallout masses in black



thermal cracking for further analyses, and weighted on a 0.01 g resolution electronic scale.

The geodata obtained were treated with a geographic information system to delimit isomass curves when possible with the help of a kriging program. The area of the isomass curves was automatically calculated to estimate the total mass of the ash fallouts using thinning laws such as exponential thinning (Pyle 1989), power law (Bonadonna and Houghton 2005), and Weibull function (Bonadonna and Costa 2012). Some of these methods require specification of the integration limits, defined as following:

- Two-segment exponential law: we searched the break of slope that gives the best coefficient of determination (R^2);
- Power law: the maximum load (L0), used to calculate the distance B, was obtained with the highest value provided by the other laws (exponential or Weibull). C is defined as the downwind limit of significant ash cloud as seen on satellite images, and it was determined using the ash dispersal limits provided by the Washington VAAC.

There were not enough isomass curves to apply three (or more) segments exponential laws. Thickness measurements were used to estimate the deposit density and volume. Based on recent research (Biass and Bonadonna 2011; Bernard et al. 2013; Engwell et al. 2013), the uncertainty on the fallout mass has been estimated between 12 and 35 % depending on sampling conditions, number of sites, wind variability, and empirical law results.

Seismic data

Cotopaxi volcano has been continuously monitored by the IGEPN since 1986. The current seismic network consists of 16 seismometers (Fig. 1c), 5 of which are vertical short period and 11 are broadband stations financed by different Ecuadorian projects (SENECYT, SENPLADES) and international collaborations (JICA, VDAP). In order to quantify the intensity of the seismic activity, we used the continuous recordings from the vertical component of station BREF, a 3-component broadband sensor, which is the closest to the summit of the volcano (~2.2 km from the crater, Fig. 1c) and away from most seismic sources such as lahars, mostly affecting the western flank since the beginning of the volcanic activity. During our study period, few explosions were seismically and acoustically recorded except on 14/08/2015 and continuous ash emission was mostly accompanied by eruption tremor. Therefore, to quantify the seismic activity, we disregarded individual transient signals and focused on estimating the amplitude of the background signal, which was mostly eruption tremor. For this purpose, we calculated median and root mean square (RMS) amplitudes over 10-min sliding windows, without overlapping, in the 0.5–5-Hz band which is the main

frequency band for signals related to venting processes such as tremor (McNutt 1992). To determine the median value of each 10-min window, we filter the seismic signal with a 4-pole Butterworth filter, calculate the absolute value of the seismic amplitudes and determine the median value of the amplitude distribution. The RMS is calculated directly in the spectral domain using the Parseval's theorem. If we apply the Discrete Fourier Transform to the unfiltered signal s_n , we get its spectrum S_k , $k = 0, 1, \dots, N-1$. The RMS of the unfiltered signal is then:

$$RMS = \frac{1}{N} \sqrt{\sum_{k=0}^{N-1} (S_k)^2} \quad (1)$$

To calculate the RMS between 0.5 and 5 Hz, we only calculate the sum over the chosen part of the spectrum. On one hand, median amplitude is particularly well suited for the quantification of long-term processes like tremor as it is little influenced by transient events. On the other hand, RMS is more sensitive to large amplitude transient signals such as regional tectonic events and instrumental problems. Therefore, we manually cleaned the temporal series to get rid of undesired events. In both cases, we directly used the raw ground velocity measurements provided by the instrument and did not correct for instrument response since we are only interested by relative temporal variations.

Results

Ash fallouts quantification

We obtained isomass maps and ash fallout masses (AFM) for 13 of the 15 sampling campaigns (Online Resources 2 and 3). The amount of ash collected during the 02/10 and 30/11 campaigns was too small ($< 10 \text{ g m}^{-2}$) to be considered significant and could have been the result of wind remobilization of ash or dust from the road. The power law method (Bonadonna and Houghton 2005) is highly sensitive to the integration limits; therefore, we only used these results for further analysis when the power law exponent (m) was ≥ 2 (campaigns 25/09 and 20/10). Three maps have only 3 isomass curves (15/08, 22/08, and 04/11), so for those only the one-segment exponential law was used for further analysis with a large uncertainty. The total masses obtained with the different empirical laws have low scattering (all $< 15 \%$) indicating a good reliability. Figure 2 shows the temporal evolution of the ash fallout compared to the median amplitude of the seismic tremor with fluctuations outlining the 4 phases of activity described above. The first phase (opening) was short-lived but intense with an average MER of ~1400 kg/s (Table 1). The second phase accumulated the highest amount of ash with a peak of activity during the

Table 1 Summary of Cotopaxi 2015 ash fallout. For the field data, the parenthesis corresponds to uncertainties on the values. For the synthetic data, the parenthesis corresponds to the date of the peaks (see Fig. 4)

Phase	Field data					Synthetic data	
	Period (dd/mm)	Mass (kg)	Volume (m ³)	Magnitude Pyle (2000)	Average MER (kg/s)	Peak daily mass of ash (kg/day)	Peak MER (kg/s)
1	14/08–15/08	1.58E + 08 (+0.45/–0.45)	1.18E + 05 (+0.33/–0.33)	1.20 (+0.11/–0.14)	1399 (+393/–393)	1.03E + 08 (14/08)	36,838 (14/08)
2	15/08–02/10	7.65E + 08 (+1.65/–1.64)	5.70E + 05 (+1.23/–1.22)	1.88 (+0.08/–0.10)	185 (+40/–39)	9.51E + 07 (28/08)	4690 (28/08)
3	02/10–04/11	2.28E + 08 (+0.57/–0.50)	1.45E + 05 (+0.36/–0.32)	1.36 (+0.10/–0.11)	80 (+20/–17)	6.36E + 07 (16/10)	3542 (14/10)
4	04/11–30/11	3.49E + 07 (+0.63/–0.62)	2.21E + 04 (+0.40/–0.39)	0.54 (+0.07/–0.08)	15 (+3/–3)	8.60E + 06 (18/11)	874 (19/11)
Global	14/08–30/11	1.19E + 09 (+0.27/–0.27)	8.59E + 05 (+1.97/–1.92)	2.08 (+0.09/–0.11)	127 (+29/–28)	1.03E + 08 (14/08)	36,838 (14/08)

MER mass eruption rate

last week of August. The third and fourth phases show a progressive decrease of the emissions both in mass and rate.

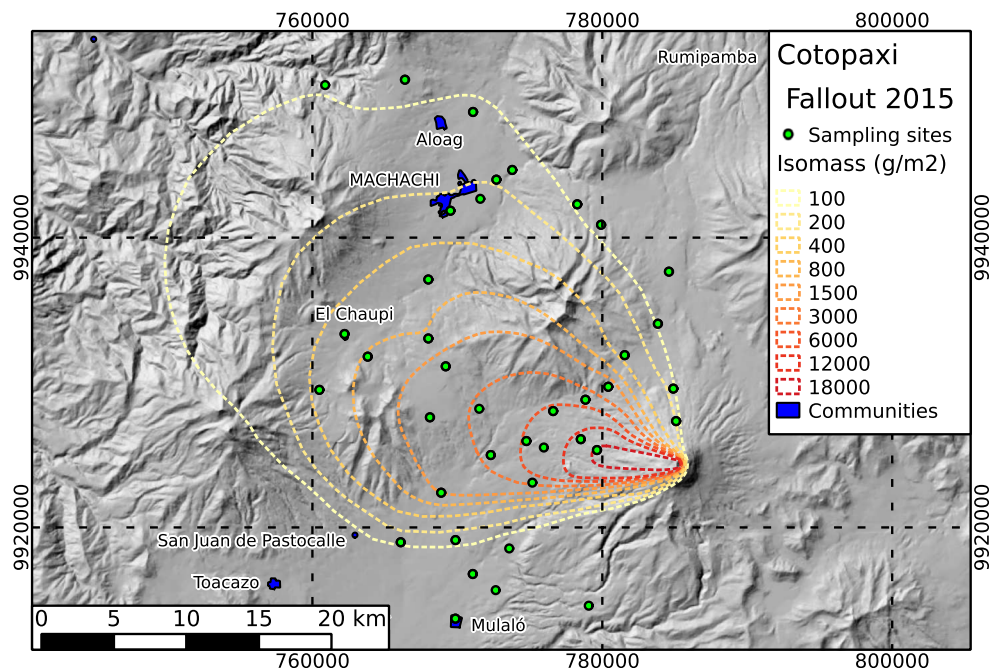
During the second and third phases, thickness measurements allowed us to estimate average dry deposit densities of $1343 \pm 128 \text{ kg m}^{-3}$ (average of 12 measurements with standard deviation) and $1572 \pm 263 \text{ kg m}^{-3}$ (6 measurements), respectively. This difference in density is probably associated with a higher compaction of the deposit due to heavy rainfalls during October, as the ash characteristics (extremely fine grain-size distribution, andesitic composition and low vesicularity, Gaunt et al. 2016, submitted to J Volcanol Geotherm Res) did not change enough to account for such a difference. We attribute similar deposit densities for the first two phases and the last two phases respectively as being due to constant atmospheric

conditions. In total, during the 14/08–30/11 period, Cotopaxi volcano accumulated $\sim 1.2E + 9 \text{ kg}$ of ash ($\sim 8.6E + 5 \text{ m}^3$) with the main dispersal axis toward the west-northwest (Fig. 3).

Ash fall-seismic data correlation

In order to compare the seismic records and the AFMs, we calculated the cumulative seismic amplitudes (both median and RMS) over the corresponding sampling intervals. Battaglia et al. (2005) used linear and quadratic relations to link the source amplitude of eruption tremor recorded at Piton de la Fournaise volcano with the amounts of basaltic lava erupted. In the present case, we use the amplitude of tremor at BREF station as a proxy to the source amplitude of tremor.

Fig. 3 Synthetic ash fallout map from the 2015 Cotopaxi eruption. This map was created compiling the data from 15 field campaigns in a geographic information system and using a Kriging program



The underlying assumption is that the tremor source location is stable, since changes in the source-station distance may affect the representativeness of the amplitude recorded at BREF station regarding the source processes. For comparison, we plotted the AFM of each campaign against the different corresponding cumulative seismic amplitude and calculated linear regressions (Fig. 4). We use the coefficient of determination (R^2) and the intercept of the linear regression equation to assess the quality of the correlation. R^2 close to 1 and small intercepts imply a proportional relationship between the variables. We compared the AFMs with different cumulative amplitudes: median amplitudes, quadratic median amplitudes (QMA), RMS, and quadratic RMS for cleaned (deglitched) data series. We also divided the global dataset according to the eruptive phases with more than 1 data point. The full set of correlation diagrams has been included in the online resource 4. These show that (1) better correlations are obtained when separating the processing into phases, (2) median amplitudes give better results than RMS, and (3) similarly to Battaglia et al. (2005) quadratic relations provides better linear regressions. Additionally, we note that the use of “glitched” time series provides poor results especially when using the quadratic RMS amplitude.

Accordingly, we choose to use the AFM/cumulative QMA relationship that gives the best fit. The regression obtained using all field campaigns (Fig. 4a) has a relatively good coefficient of determination ($R^2 = 0.81$) but a large positive intercept ($+3.7E + 7$ kg). For the opening phase (only one data point), the ratio AFM/cumulative

QMA is ~ 26.7 . We found regressions with excellent ($R^2 \geq 0.97$) correlations for the second and third phases (Fig. 4b, c). The intercept values for these correlations are smaller by a factor of 17 and 10 respectively compared to the global correlation. Although the regression for the fourth phase (Fig. 4d) only has two data points, generating a R^2 of 1, the small intercept ($+5.7E + 6$ kg, 6 times smaller compared to the global correlation) and the positive slope suggest a good correlation between seismic tremor and ash fallout for this phase. The slopes of the linear regressions appear to increase through time going from 1.1 for the second phase, 7.7 for the third, to 9.6 for the fourth. As the intercept for these linear regressions is very small and their R^2 is excellent, their slope can be used as a scaling factor between the QMA and the ash emission rate.

Extraction of Eruption Source Parameters from the seismic records

Daily mass of ash

A synthetic time series was calculated for the emitted mass of ash by multiplying the continuous QMA by the scaling factors established for each phase (Fig. 5a, online resource 5). The difference between the synthetic and the real fallout mass is extremely small ($\sim 0.3\%$). As a comparison, the use of the global correlation would lead to an underestimation of the ash mass of

Fig. 4 Correlation between the cumulative quadratic median amplitude (cumulative QMA) of the seismic tremor and the ash fallout mass (AFM) for **a** all the field campaigns, **b** phase 2, **c** phase 3, **d** phase 4

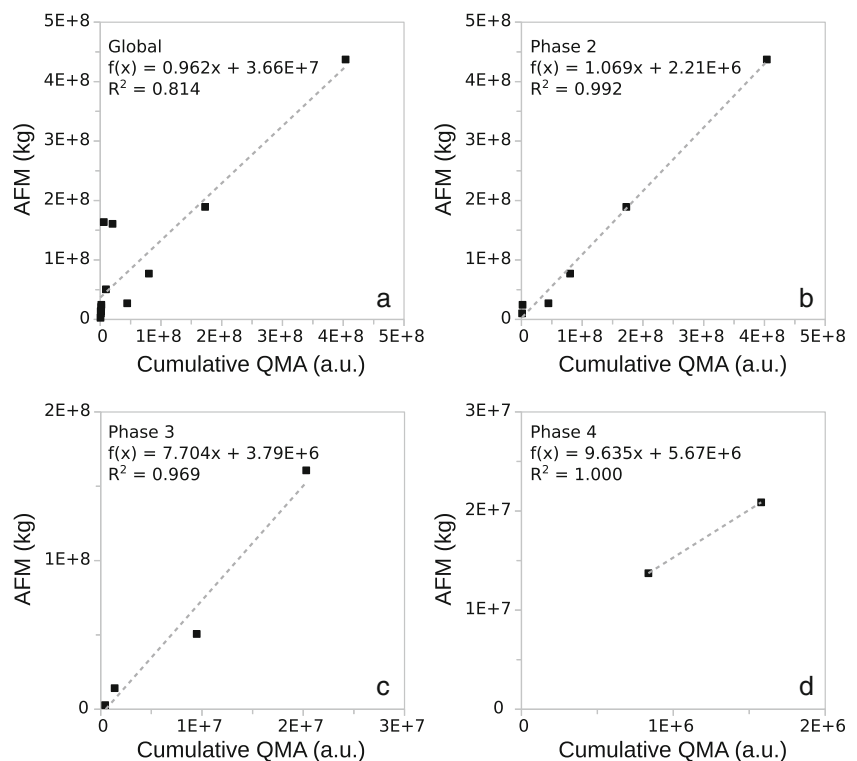
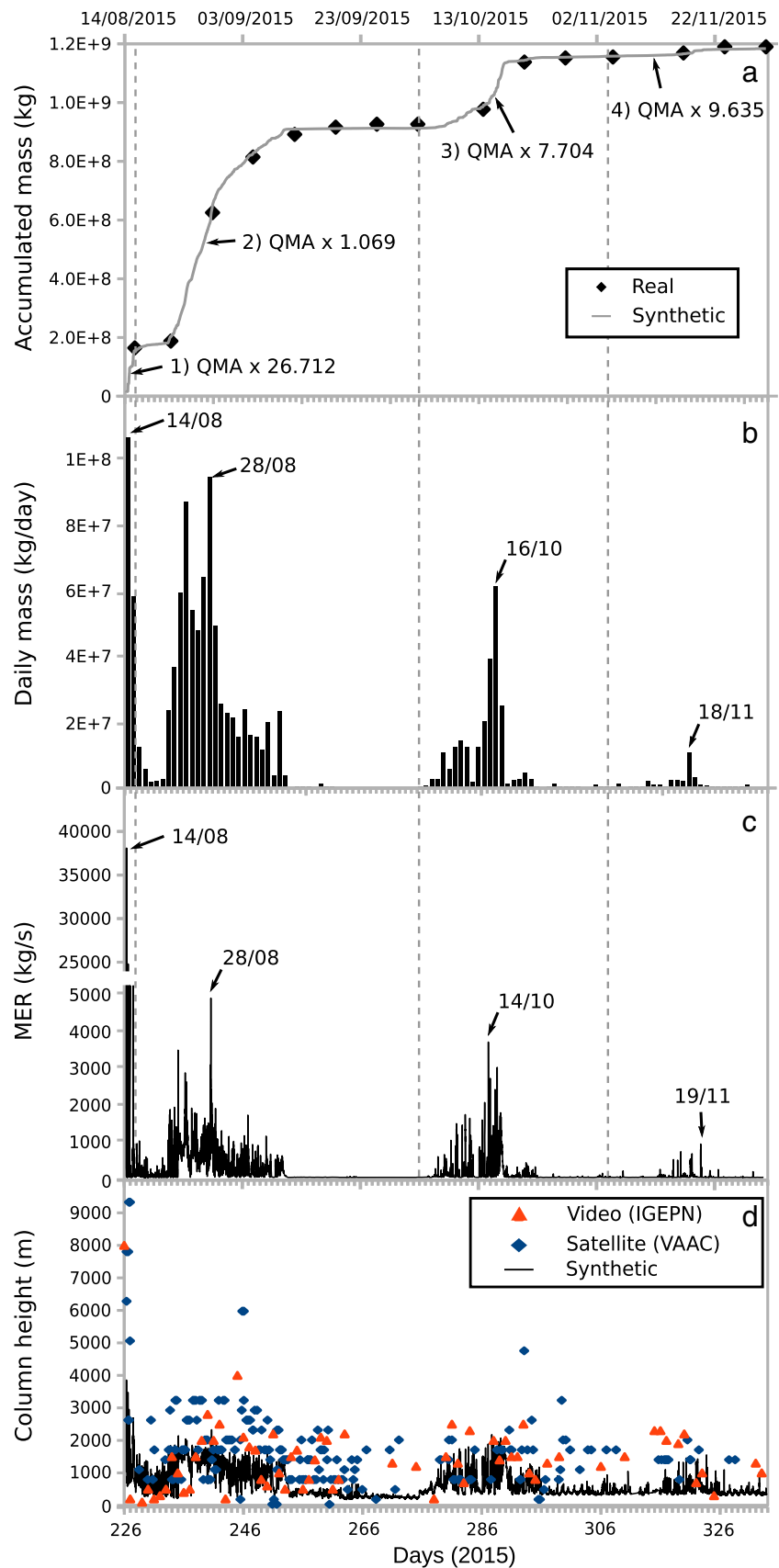


Fig. 5 **a** Comparison between the real cumulative fallout mass (black diamonds) and the synthetic cumulative fallout mass (continuous gray line) created using the quadratic median amplitude (QMA) and the scaling factors by phase. **b** Daily ashgram for the whole eruption with the date of each peak of ash emission indicated. **c** Synthetic mass eruption rate (MER) for the whole eruption with the date of the highest emission rates indicated for each phase. Note the break in the MER axis in order to improve the visual rendering. **d** Synthetic column height obtained using the MER and the empirical relationship from Mastin et al. (2009) compared to observations (video and satellite)



~40 %. Figure 5b is a daily ashgram, defined as a graph showing the amount of ash emitted per day. This ashgram allows to identify and quantify the days with the highest amount of ash during the different eruptive phases (Table 1). The amounts of ash calculated for the two periods without fallout quantification (25/09–02/10 = $4.2E + 5$ kg; 23/11–30/11 = $2.2E + 6$ kg) are very small and inferior to the minimum mass registered for the 04/11 sampling campaign ($2.8E + 6$ kg). It is interesting to note that daily masses of ash calculated using the median amplitudes are far less sensitive (<10 %) to the occurrence of external events as compared to the RMS which may lead to significant error when using raw data (up to >100 %).

Mass eruption rate

The continuous QMA allows us to calculate a synthetic MER from the 10-min windows (Online Resource 5). In Fig. 5c, we present the continuous synthetic MER that illustrates the intensities during the different phases of the eruption and highlights the pulsatile behavior of the ash emissions. This pulsatile behavior tends to increase for the third and fourth phases being coincident with the increase in occurrence of small transient events detected by seismo-acoustic sensors without superficial evidence such as ballistic projectiles nor individual ash or gas columns. The synthetic MER is much more sensitive to external events for both QMA and quadratic RMS time series; therefore, rejection of external events is mandatory to adequately extract continuous MER estimates from the seismic records. As for the daily mass of ash, this method allows us to identify the highest MER recorded during the different eruptive phases (Table 1, Fig. 5).

Column height

The MER can be used to calculate the height of the eruptive column using the statistical relationship established by Mastin et al. (2009):

$$H = 2.00V^{0.241} \quad (2)$$

where H is the column height (in km) and V , the volumetric flow rate (m^3/s), is obtained dividing the MER by the density of the equivalent magma (assumed 2500 kg m^{-3} for an andesitic composition).

The synthetic column heights obtained (online resource 5) tend to be smaller than those measured by satellite, but close to those obtained using video cameras (Fig. 5d). The difference between modeled and observed column heights could be due to the plume characteristics (buoyancy, ash concentration, exit velocity), atmospheric characteristics (stratification, temperature, and pressure profiles), and also data temporal resolution (Sparks et al. 1997, Bursik 2001, Devenish 2013). Nevertheless, the resulting synthetic data series is globally coherent with the observations.

Discussion

Size and phenomenology of the 2015 Cotopaxi eruption

The determination of the size of a volcanic eruption is crucial for hazard assessment. Based on the amount of ash emitted by Cotopaxi volcano, the 2015 eruption can be classified as a magnitude 2.1 (Pyle 2000) with the different phases ranging from magnitude 0.5 to 1.9 (Table 1). The Volcanic Explosivity Index (Newhall and Self 1982, Houghton et al., 2013) is a semi-quantitative classification based on various parameters where the most important one is the volume of ejecta. Accordingly, the 2015 Cotopaxi eruption should be ranked VEI 1–2 when including the uncertainty on the volume estimate. A VEI 2 would be more coherent with the observed column height during the whole eruption (1–5 km high) except for the first day when the eruptive column reached 9.3 km above the crater. Compared to historical and Holocene records (Hall and Mothes 2008; Pistolesi et al. 2011), this eruption is 2 to 3 order of magnitude smaller than the moderate-large eruptions at Cotopaxi. Such eruption size is probably frequent at Cotopaxi according to the Global Volcanism Program (<http://volcano.si.edu>) but has not been quantified before due to the lack of deposit in the geological records.

During the 2015 Cotopaxi eruption, ash emission was the primary volcanic phenomenon observed. Apart from the first day of the eruption, no superficial explosion was observed but, during the third and fourth emission phases, transient events were recorded by seismo-acoustic sensors. These events might have influenced the pulsatile behavior of the ash emission during those late eruptive phases. Also, throughout the eruption, the eruptive column was mostly cold (<200 °C) according to the airborne IR imagery obtained since the 15/08 (IGEPN special report n°14, 05/09/2015) and continuous ground-based IR camera installed the 15/09. Therefore, it is likely that the fragmentation source remained deep inside the conduit during the eruption. The first explosions opened the conduit and ash venting was the dominant process from there, driven by a high gas flux and associated with intense seismic tremor.

Relationship between seismic tremor and ash fallout

Finding and understanding relationships between geophysical/geochemical data and eruptive source parameters is crucial to improve hazard assessment and reduce the negative effects of volcanic eruptions (Sparks 2003). The relationship between seismic tremor and Eruption Source Parameters through eruptive phases has been explored mostly for lava output (Alparone et al. 2003; Battaglia et al. 2005; Coppola et al. 2009; Hibert et al. 2015). The relationship between seismic tremor and VEI has also been explored (McNutt 1994; McNutt 2005) but as VEI is a non-continuous pseudo-logarithmic scale, the resulting correlations remain vague. McNutt and Nishimura (2008) found a

correlation between seismic tremor and vent area and conclude that this parameter is more important than flow velocity in controlling the mass flux. Consequently, they state that, in principle, the eruption discharge rate could be monitored using tremor amplitude. Andronico et al. (2009) qualitatively describe the correlation between seismic and eruptive activity during the 16 November 2006 Etna eruption and propose that the high intensity of the seismic tremor compared to low amounts of ash produced could indicate a high gas/magma ratio during the paroxysmal phase. Kumagai et al. (2015) found that inharmonic tremor better correlates with the amount of ash emitted than harmonic tremor at Tungurahua volcano and propose that the cumulative source amplitudes may be used as a measure of total ejecta mass during an eruptive phase. Our results indicate a proportional relationship between the cumulative quadratic median amplitude (QMA) of the seismic tremor and the ash fallout mass (AFM), in good agreement with Kumagai et al. (2015) and McNutt and Nishimura conclusions but outlining the quadratic nature of this relationship. Our statistical analysis also shows that this proportionality is not unique and can vary from one eruptive phase to another. Andronico et al. (2013) also found two kinds of ash emissions at Etna volcano based on seismo-acoustic signals and associated them with different conduit conditions. At Cotopaxi, between the second, third, and fourth eruptive phases, the slope of the linear regressions systematically increases, outlining a decreasing tremor amplitude associated with ash emissions. This observation could indicate a more efficient fragmentation and transport process. This could also be related to differences in the eruptive dynamics (hydromagmatic vs. magmatic fragmentation, gas/magma ratio, depth of the fragmentation, cleanliness and radius of the conduit) that should be investigated through textural and componentry analysis of the ash sample, seismic source location, acoustic-seismic ratio, and gas emission analysis that are beyond the scope of this paper. A practical use of such correlations for monitoring teams would be to use the Eq. (2) to estimate the MER when eruptive plumes are observed. Comparing this MER with the seismic tremor would allow to calculate the scaling factor if a correlation is obtained. This scaling factor could be used to estimate the MER and column height when the volcano is cloudy and to calculate the cumulative mass of ash emitted. The scaling factor should then be refined using the results of new sampling campaigns. This empirical method could be coupled with volcanic acoustic-seismic ratio in order to track conduit conditions and characterize eruptive dynamics (Johnson and Aster 2005).

Origin of the pre-eruptive tremor

The seismic tremor at Cotopaxi started about 2 months before the beginning of the eruption (Fig. 2), on June 4, and was then associated with SO₂ emissions (Hidalgo et al. 2016). There is no clear difference in the frequency content of the seismic tremor before and after the start of the eruption, so their origin could be

similar and linked to outgassing. If most of the fragmentation during a volcanic eruption is either due to rapid acceleration associated to volatile exsolution and vesiculation processes or to rapid decompression (McNutt 1992; Cashman and Scheu 2015), then we can presume that those processes also occurred during the pre-eruptive phase at Cotopaxi producing the increase of seismic tremor amplitude observed but, due to decades of inactivity, the fragmented material could not reach the surface because the vent was closed. An alternative, and potentially complementary, hypothesis would be that the pre-eruptive tremor was generated by the boiling of the hydrothermal system due to a magmatic intrusion and consequently produced hydromagmatic fragmentation. In this hypothesis, once the eruption started, the evolution of the linear regression's slope toward a more efficient fragmentation and transport process could be interpreted as the drying out or insulation of the hydrothermal system around the intrusion and the cleaning of the volcano conduit. A conduit filled by fragmented material during the pre-eruptive period could explain the high AFM/cumulative QMA ratio calculated for the opening phase.

Conclusion

In this paper, we present the first quantification of the 2015 ash fallouts at Cotopaxi volcano based on a high-frequency sampling. This eruption emitted a total of $\sim 1.2E + 9$ kg of ash ($\sim 8.6E + 5$ m³) during 4 eruptive phases and thus has a magnitude of 2.1 and a VEI of 2 (taking into account the column height and the uncertainty on the volume estimate). We explored the relationship between the intense seismic tremor recorded during the eruption and the ash fallout mass (AFM) and found that, among 4 different amplitude-measurement techniques, seismic tremor is best quantified using Quadratic Median Amplitudes (QMA). The AFM/cumulative QMA correlations improve significantly when the dataset is divided by eruptive phase, highlighting the temporally heterogeneous behavior of the volcanic system. Based on these results, it was possible to extract synthetic eruptive source parameters (daily mass of ash, MER, plume height) from the seismic records using empirically derived scaling factors. Extraction of these parameters from a continuous monitoring system could help real-time hazard assessment, but our study shows that calibrations based on high-frequency field sampling are necessary. Accordingly, volcanic ash transport and dispersal models could be fed continuously by the synthetic MER and plume height in order to improve ash plume dispersal forecasts but, in order to avoid errors, it requires cleaning the data series of external events such as regional earthquakes. Finally, our analysis of the correlations indicates that some important changes in the eruptive dynamics probably occurred over the course of the eruption that should be investigated using textural analysis of the ash particles, seismic source location, and gas emission analysis.

Acknowledgments Field campaigns for this study were funded by the project SENPLADES. Seismic data came from the JICA seismic network. This research has been conducted in the context of the Laboratoire Mixte International “Séismes et Volcans dans les Andes du Nord” of IRD. This work is the contribution n°2 of the project “Grupo de Investigación sobre la Ceniza Volcánica en Ecuador”. The authors thank the personnel of IGEPN, in particular those who participated to the field campaigns. Comments from D. Pyle, T. Nishimura, and an anonymous reviewer greatly improved a first version of this paper. We thank two anonymous reviewers and J. Taddeucci for their constructive comments which helped improving this paper.

References

- Alparone S, Andronico D, Lodato L, SgROI T (2003) Relationship between tremor and volcanic activity during the southeast crater eruption on Mount Etna in early 2000. *J Geophys Res-Sol Ea* 108(B5): 2241. doi:10.1029/2002JB001866
- Andronico D, Scollo S, Cristaldi A, Ferrari F (2009) Monitoring ash emission episodes at Mt. Etna: the 16 November 2006 case study. *J Volcanol Geoth Res* 180(2–4):123–134. doi:10.1016/j.jvolgeores.2008.10.019
- Andronico D, Lo Castro MD, Sciotto M, Spina L (2013) The 2010 ash emissions at the summit craters of Mt Etna: relationship with seismo-acoustic signals. *J Geophys Res Solid Earth* 118:51–70. doi:10.1029/2012JB009895
- Battaglia J, Aki K, Ferrazzini V (2005) Location of tremor sources and estimation of lava output using tremor source amplitude on the piton de la fournaise volcano: 2. Estimation of lava output. *J Volcanol Geoth Res* 147:291–308
- Bernard B (2013) Homemade ashmeter: a low-cost, high-efficiency solution to improve tephra field-data collection for contemporary explosive eruptions. *J Appl Volcanol* 2(1): 1–9. doi:10.1186/2191-5040-2-1
- Bernard B, Bustillos J, Wade B, Hidalgo S (2013) Influence of the wind direction variability on the quantification of tephra fallouts: December 2012 and march 2013 Tungurahua eruptions. *Avances en Ciencias e Ingenierías* 5(1):A14–A21
- Biass S, Bonadonna C (2011) A quantitative uncertainty assessment of eruptive parameters derived from tephra deposits: the example of two large eruptions of Cotopaxi volcano, Ecuador. *Bull Volcanol* 73(1):73–90
- Bonadonna C, Costa A (2012) Estimating the volume of tephra deposits: a new simple strategy. *Geology* 40(5):415–418. doi:10.1130/G32769.1
- Bonadonna C, Houghton BF (2005) Total grain-size distribution and volume of tephra-fall deposits. *Bull Volcanol* 67:441–456
- Bonadonna C, Folch A, Loughlin S, Puempel H (2012) Future developments in modelling and monitoring of volcanic ash clouds: outcomes from the first IAVCEI-WMO workshop on ash dispersal forecast and civil aviation. *Bull Volcanol* 74(1): 1–10. doi:10.1007/s00445-011-0508-6
- Bursik M (2001) Effect of wind on the rise height of volcanic plumes. *Geophys Res Lett* 28:3621–3624. doi:10.1029/2001GL013393
- Caplan-Auerbach J, Bellesiles A, Fernandes JK (2010) Estimates of eruption velocity and plume height from infrasonic recordings of the 2006 eruption of Augustine volcano, Alaska. *J Volcanol Geoth Res* 189(1–2):12–18. doi:10.1016/j.jvolgeores.2009.10.002
- Cashman KV, Scheu B (2015) Magmatic fragmentation. In: Sigurdsson H (ed) *The encyclopedia of volcanoes*, 2nd edn. Academic Press, Amsterdam, p 459–471
- Collini E, Osoro MS, Folch A, Viramonte JG, Villarosa G, Salmuni G (2012) Volcanic ash forecast during the June 2011 cordón caulle eruption. *Nat Hazards* 66(2):389–412. doi:10.1007/s11069-012-0492-y
- Connor CB, Hill B, Winfrey B, Franklin N, La Femina PC (2001) Estimation of volcanic hazards from tephra fallout. *Nat Hazards Rev* 2(1):33–42. doi:10.1061/(ASCE)1527-6988(2001)2:1(33)
- Coppola D, Piscopo D, Staudacher T, Cigolini C (2009) Lava discharge rate and effusive pattern at piton de la fournaise from MODIS data. *J Volcanol Geoth Res* 184(1–2):174–192. doi:10.1016/j.jvolgeores.2008.11.031
- Costa A, Macedonio G, Folch A (2006) A three-dimensional Eulerian model for transport and deposition of volcanic ashes. *Earth Planet Sci Lett* 241(3–4):634–647. doi:10.1016/j.epsl.2005.11.019
- Devenish BJ (2013) Using simple plume models to refine the source mass flux of volcanic eruptions according to atmospheric conditions. *J Volcanol Geotherm Res.* doi:10.1016/j.jvolgeores.2013.02.015
- Donnadieu F (2012) Volcanological applications of doppler radars: A review and examples from a transportable pulse radar in L-Band. In: Bech J (ed) *Doppler radar observations—weather radar, wind profiler, ionospheric radar, and other advanced applications*. InTech
- Donnadieu F, Freville P, Hervier C, Coltelli M, Scollo S, Prestifilippo M, Valade S, Rivet S, Cacault P (2016) Near-source Doppler radar monitoring of tephra plumes at Etna. *J Volcanol Geotherm Res* 312:26–39. doi:10.1016/j.jvolgeores.2016.01.009
- Dürig T, Gudmundsson MT, Karmann S, Zimanowski B, Dellino P, Rietze M, Büttner R (2015) Mass eruption rates in pulsating eruptions estimated from video analysis of the gas thrust-buoyancy transition—a case study of the 2010 eruption of Eyjafjallajökull, Iceland. *Earth Planets Space* 67:1–17. doi:10.1186/s40623-015-0351-7
- Engwell SL, Sparks RSJ, Aspinall WP (2013) Quantifying uncertainties in the measurement of tephra fall thickness. *J Appl Volcanol* 2(1):1–12. doi:10.1186/2191-5040-2-5
- Hall M, Mothes P (2008) The rhyolitic-andesitic eruptive history of Cotopaxi volcano, Ecuador. *Bull Volcanol* 70(6):675–702. doi:10.1007/s00445-007-0161-2
- Hibert C, Mangeny A, Polacci M, Muro AD, Vergnolle S, Ferrazzini V, Peltier A, Taisne B, Burton M, Dewez T, Grandjean G, Dupont A, Staudacher T, Brenguier F, Kowalski P, Boissier P, Catherine P, Lauret F (2015) Toward continuous quantification of lava extrusion rate: results from the multidisciplinary analysis of the 2 January 2010 eruption of piton de la fournaise volcano, La Réunion. *J Geophys Res-Sol Ea* 120(5):2014JB011769. doi:10.1002/2014JB011769
- Hickey J, Gottsmann J, Mothes P (2015) Estimating volcanic deformation source parameters with a finite element inversion: the 2001–2002 unrest at Cotopaxi volcano, Ecuador. *J Geophys Res-Sol Ea* 120(3):2014JB011731. doi:10.1002/2014JB011731
- Hidalgo S, Bernard B, Battaglia J, Gaunt E, Barrington C, Andrade D, Ramón P, Arellano S, Yepes H, Proaño A, Almeida S, Sierra D, Dinger F, Kelly P, Parra R, Bobrowski N, Galle B, Almeida M, Mothes P, Alvarado A, IGEPN (2016) Cotopaxi volcano’s unrest and eruptive activity in 2015: Mild awakening after 73 years of quiescence. In: Abstract volume of the 2016 EGU General Assembly. p EGU2016–5043-1
- Houghton BF, Swanson DA, Rausch J, Carey RJ, Fagents SA, Orr TR (2013) Pushing the volcanic explosivity index to its limit and beyond: constraints from exceptionally weak explosive eruptions at Kilauea in 2008. *Geology* v 41:627–630. doi:10.1130/G34146.1
- Jenkins SF, Wilson TM, Magill CR, Miller V, Stewart C, Marzocchi W, Boulton M (2015) Volcanic ash fall hazard and risk: Technical background paper for the UNISDR 2015 global assessment report on disaster risk reduction. Global volcano model and IAVCEI
- Johnson JB, Aster RC (2005) Relative partitioning of acoustic and seismic energy during Strombolian eruptions. *J Volcanol Geoth Res* 148:334–354. doi:10.1016/j.jvolgeores.2005.05.002

- Kratzmann DJ, Carey SN, Fero J, Scasso RA, Naranjo J (2010) Simulations of tephra dispersal from the 1991 explosive eruptions of Hudson volcano, Chile. *J Volcanol Geoth Res* 190(3–4):337–352. doi:10.1016/j.jvolgeores.2009.11.021
- Kumagai H, Mothes P, Ruiz M, Maeda Y (2015) An approach to source characterization of tremor signals associated with eruptions and lahars. *Earth Planets Space* 67(1):178. doi:10.1186/s40623-015-0349-1
- Mastin LG, Guffanti M, Servranckx R, Webley P, Barsotti S, Dean K, Durant A, Ewert JW, Neri A, Rose WI, Schneider D, Siebert L, Stunder B, Swanson G, Tupper A, Volentik A, Waythomas CF (2009) A multidisciplinary effort to assign realistic source parameters to models of volcanic ash-cloud transport and dispersion during eruptions. *J Volcanol Geoth Res* 186(1–2):10–21. doi:10.1016/j.jvolgeores.2009.01.008
- Matoza RS, Fee D, Neilsen TB, Gee KL, Ogden DE (2013) Aeroacoustics of volcanic jets: acoustic power estimation and jet velocity dependence. *J Geophys Res Solid Earth* 118:6269. doi:10.1002/2013JB010303
- McNutt SR (1992) Volcanic tremor, in encyclopedia of earth system science. Academic Press, San Diego, California, pp. 417–425
- McNutt SR (1994) Volcanic tremor amplitude correlated with Volcanic Explosivity Index and its potential use in determining ash hazards to aviation. *Acta Vulcanol* 5:193–196
- McNutt SR (2005) Volcanic seismology. *Annu Rev Earth Planet Sci* 32: 15.1–15.31. doi:10.1146/annurev.earth.33.092203.122459
- McNutt SR, Nishimura T (2008) Volcanic tremor during eruptions: temporal characteristics, scaling and constraints on conduit size and processes. *J Volcanol Geotherm Res* 178:10–18. doi:10.1016/j.jvolgeores.2008.03.010
- Molina I, Kumagai H, García-Aristizábal A, Nakano M, Mothes P (2008) Source process of very-long-period events accompanying long-period signals at Cotopaxi volcano, Ecuador. *J Volcanol Geoth Res* 176(1):119–133. doi:10.1016/j.jvolgeores.2007.07.019
- Newhall CG, Self S (1982) The volcanic explosivity index (VEI): an estimate of explosive magnitude for historical volcanism. *J Geophys Res* 87(C2):123–1238
- Parra R, Bernard B, Narváez D, Le Pennec J-L, Hasselle N, Folch A (2016) Eruption source parameters for forecasting ash dispersion and deposition from vulcanian eruptions at Tungurahua volcano: insights from field data from the July 2013 eruption. *J Volcanol Geoth Res* 309:1–13. doi:10.1016/j.jvolgeores.2015.11.001
- Pistolesi M, Rosi M, Cioni R, Cashman KV, Rossotti A, Aguilera E (2011) Physical volcanology of the post-twelfth-century activity at Cotopaxi volcano, Ecuador: behavior of an andesitic central volcano. *Geol Soc Am Bull* 123(5–6):1193–1215. doi:10.1130/B30301.1
- Prejean SG, Brodsky EE (2011) Volcanic plume height measured by seismic waves based on a mechanical model. *J Geophys Res* 116: B01306. doi:10.1029/2010JB007620
- Pyle DM (1989) The thickness, volume and grainsize of tephra fall deposits. *Bull Volcanol* 51:1–15
- Pyle DM (2000) Sizes of volcanic eruptions. In: Sigurdsson H, Houghton BF, McNutt SR, Rymer H, Stix J (eds) *Encyclopedia of volcanoes*. Academic Press, London, pp. 263–270
- Ripepe M, Bonadonna C, Folch A, Delle Donne D, Lacanna G, Marchetti E, Höskuldsson A (2013) Ash-plume dynamics and eruption source parameters by infrasound and thermal imagery: the 2010 Eyjafjallajökull eruption. *Earth Planet Sci Lett* 366:112–121. doi:10.1016/j.epsl.2013.02.005
- Ruiz M, Guillier B, Chatelain J-L, Yepes H, Hall M, Ramon P (1998) Possible causes for the seismic activity observed in Cotopaxi volcano, Ecuador. *Geophys Res Lett* 25:2305–2308
- Sparks RSJ (2003) Forecasting volcanic eruptions. *Earth Planet Sci Lett* 210(1–2):1–15. doi:10.1016/S0012-821X(03)00124-9
- Sparks RSJ, Bursik MI, Carey SN, Gilbert JS, Glaze LS, Sigurdsson H, Woods AW (1997) *Volcanic plumes*. John Wiley & Sons, Chichester